J Mater Sci (2008) 43:4455–4465
DOI 10.1007/s10853-008-2655-5

New type of low-dielectric composites based on *o*-cresol novolac epoxy resin and mesoporous silicas: fabrication and performances

Jingjing Lin · Xiaodong Wang

Received: 23 December 2007 / Accepted: 14 April 2008 / Published online: 29 April 2008

Abstract A series of *o*-cresol novolac epoxy (*o*-CNER)-based composites containing various amount of SBA-15, SBA-16, and MSU-X type mesoporous silicas were prepared, and their performances were evaluated. Morphological investigation by SEM reveals that the mesoporous silicas achieve a good dispersion in the *o*-CNER matrix due to an effective surface modification. The dielectric constants of all the composites were measured in the frequency range of 50–1,000 kHz. The investigation suggested that the dielectric constant could be reduced from 4.0 of the pure thermosetting *o*-CNER to 3.71, 3.73, and 3.73 by incorporating 5 wt.% SBA-15, SBA-16, and MSU-X, respectively. The reduction is attributed to incorporation of air voids stored within the mesoporous silicas, the air volume existing in the gaps on interfaces between the mesoporous silica and the matrix, and the free volume created by introducing large-sized domains. The composites present stable dielectric constants across the wide frequency range. An improvement of thermal stability of the *o*-CNER is achieved by incorporation of the mesoporous silica materials, while the enhanced interfacial interaction between the surface-modified mesoporous silica and the *o*-CNER matrix has also led to an improvement of toughness.

J. Lin · X. Wang (✉)
Key Laboratory of Beijing City on Preparation and Processing of Novel Polymer Materials, School of Materials Science and Engineering, Beijing University of Chemical Technology, Beijing 100029, China
e-mail: wangxdfox@yahoo.com.cn

Introduction

High-performance epoxy-based composites play an important role in integrated circuit (IC) chip packaging as encapsulants, which provide chemical and mechanical protection to the IC chips, allowing higher reliability and longer lifetime of the packaged device under the adverse service environment [1]. For example, the epoxy-based composites used for sealing of integrated circuits are usually prepared by hardening *o*-cresol novolac epoxy resin (*o*-CNER) [2, 3]. Owing to the presence of multi-functionality, a three-dimensional network structure with highly crosslinking density was formed during the *o*-CNER curing. A higher degree of cross-linking endows these cross-linked resins with excellent performance. Nowadays, the *o*-CNER-based composites have been used as one of the most important packaging materials in the field of microelectrics and semiconductor manufacture [4]. Through introducing suitable reinforcing fillers such as silicon dioxide, organomontmorillonite, etc., the properties of the *o*-CNER-based composites can be tailored to meet specific design requirements such as low density, high strength, high damping, thermal shock resistance, high thermal conductivity, low coefficient of thermal expansion, and good electrical properties, so that they can cope with the trend of the IC ships toward greater integration and functionality placing a great challenge on the basic resins for encapsulation [5, 6]. Several attempts have been made on the clay/*o*-CNER nanocomposites. Han and Cho [7] noticed that the fracture toughness, the storage modulus, and the glass transition temperature (T_g) of epoxy resins were dramatically improved by incorporation of the layered silicate. Gao et al. [8] studied a nanocompositing system of the *o*-CNER with organic montmorillonite (O-MMT) and found that the thermal stability was improved with an increase of the O-MMT content. Liu et al. [9] introduced the nano-scaled silica into *o*-CNER through a sol–gel

process, and obtained cured epoxy/silica composites with the high T_gs, excellent thermal stability, improved flame retardance, and low coefficient of thermal expansion.

In recent years, mesoporous silica materials have attracted considerable interest in applications of molecular sieves, catalysts, adsorbents, optical devices, and sensor devices due to their highly ordered and uniform mesoporosity [10]. Most importantly, the mesoporous silica materials synthesized in a surfactant templating process could provide large pore sizes (5–30 nm), high porosities (45–75%), and controlled pore structures [11]. This makes it possible to introduce voids into the bulk so that the low-dielectric air ($c = 1$) can be utilized to reduce the dielectric constant (c) of the materials. Many studies showed that the mesoporous silica materials have low-dielectric constants in the range of 1.42–2.1 at 1 MHz [12–14], which are lower than most of the other low-dielectric materials such as silisequioxane-based dielectric, fluorine-doped silica film, carbon-doped silica film, organic polymer dielectric, and Dow Corning's porous SiLK [15]. The low-dielectric mesoporous silica materials can meet the requirements of the new low-dielectric materials for the applications in the microelectronics and the insulations. Chen-Yang et al. [16] prepared the PTFE/MCM-41 composites broads with ultra-low-dielectric constant (1.7–2.05) at 1 MHz. Cheng et al. also reported that the mesoporous silica could reduce the dielectric constant of polyimde, though the results had different variation trend with results as we reported [17, 18]. Wang et al. [19] prepared the epoxy resin/MCM-41composites, but did not investigate the dielectant constant. Therefore, incorporation of the mesoporous silica materials into the epoxy resins would be expected to reduce the dielectric constants of the epoxy resins.

In present work, we reported a new approach to prepare the *o*-CNER-based composites by incorporating the mesoporous silicas into the resin matrix to combine the low-dielectric constant of mesoporous silicas and the excellent properties of the *o*-CNER. A significant reduction of the dielectric constants for the *o*-CNER-based composites can be achieved by this method. We also evaluate the effects of the mesoporous silica materials on the *o*-CNER-based composites in terms of the dielectric and thermal properties. The present work provides a simple and effective means to obtain the low-dielectric epoxy-based composites.

Experimental

Materials

Poly(ethylene oxide–*b*–propylene oxide–*b*–ethylene oxide) (EO_n–PO_m–EO_n) triblock copolymers, EO_{20}–PO_{70}–EO_{20} (Pluronic P123), EO_{106}–PO_{70}–EO_{106} (Pluronic F127), and EO_{27}–PO_{61}–EO_{27} (Pluronic P104) were commercially obtained from BASF Company. Tetraethoxysilane (TEOS) used as silica source and 3-glycidyl oxypropyl trimethoxysilane (GOTMS) used as coupling agent were purchased from Aldrich Chemical Company. The *o*-CNER (EPICLON® N-670) with an epoxide equivalent weight of 200–230 g $eq.^{-1}$ was kindly supplied by Wuxi Dic Epoxy Co., Ltd. 3-Methyl-tetrahydrophthalic anhydride (MeTHPA) and 2-methyl imidazole were purchased from Beijing Chemical Reagent Company. All chemicals were of reagent quality and used as received without further purification.

Synthesis of mesoporous silicas

Three types of the mesoporous silicas, SBA-15, SBA-16, and MXU-X, were synthesized respectively by using the EO_{20}–PO_{70}–EO_{20}, EO_{106}–PO_{70}–EO_{106}, and EO_{27}–PO_{61}–EO_{27} surfactants as templates in a sol–gel process. A typical synthesis was carried out as follows [20–22]: the amount of surfactant template was dissolved in deionized water with stirring in a beaker at 35 °C to form a transparent template solution containing the surfactant micelles. In another beaker, a mixture of the amount of TEOS and aqueous HCl solution required to give the desired pH was stirred at 35 °C until a homogeneous solution was obtained, indicating that the hydrolysis of the TEOS was complete. Then, the above two solutions were mixed with stirring for 24 h. In succession, the mixture was aged at 100 °C for another 24 h. The solid powers were collected by filtration, washed with water, and dried at room temperature in air. The resulting products were calcined at 500 °C for 5 h to remove the template.

Preparation of *o*-CNER/mesoporous silica composites

The mesoporous silicas were first surface modified with coupling agent before use in the following way: The mesoporous silicas were dispersed in dry acetone under ultrasonic agitation for 30 min, and then the calculated amount of GOTMS was added to the mixture with loading of 0.5 wt.%, refluxed 12 h under vigorous stirring. After the mixture was filtrated with Buchner funnel, the product was washed several times using acetone and dried in the vacuum oven at room temperature.

The *o*-CNER/mesoporous silicas were prepared as follows: the *o*-CNER was dissolved in acetone in a beaker. The calculated amount of mesoporous silica was dispersed in the solution under ultrasonic agitation in another beaker for 30 min, and then the MeTHPA as curing agent and the 2-methyl imidazole as catalyst were added into this beaker. The above two solutions were mixed with stirring for 30 min. Then, the solvent was removed at 50 °C under

0.05 MPa pressure in a vacuum oven. Subsequently, the mixture was poured into the preheated molds, which were surface treated with the mold-releasing agent. All the samples were cured at 100 °C for 1 h and at 178 °C for 2 h.

Characterizations

X-ray powder diffraction (XRD) was carried out with a Rigaku D/max-r C diffractometer (40 kV, 50 mA) with Cu-Kα radiation ($\lambda = 0.154$ nm), the diffraction patterns being collected in the 2θ range 0.5–8.0° at a scanning rate of 0.2° min^{-1}. Transmission electron microscopy (TEM) images were obtained by a Hitachi H-800 transmission electron microscope operating at 200 kV. Samples for TEM observation were prepared by dispersing a drop of a suspension of a ground sample in ethanol on a copper grid covered by carbon film. N_2 adsorption–desorption isotherms were obtained at 77 K using a Nova 4200e gas-adsorption analyzer. Before the adsorption measurements, the samples were degassed under vacuum at 200 °C for 12 h. The mean pore diameter and the diameter distribution were calculated from the adsorption branch of the isotherm using the Barrett–Joyner–Halenda (BJH) method. The specific surface area was calculated using the Brunauer–Emmett–Teller (BET) model. Fourier transform IR (FTIR) spectra of the mesoporous silicas and the surface-modified ones were obtained using a Bruker Tensor-27 FTIR spectrometer with 30 scans. Scanning electron microscopy (SEM) observation was performed on a Hitachi S-4700 SEM. The morphologies of the mesoporous silica powders and the fracture surfaces of the *o*-CNER/mesoporous silica composites were determined from SEM images. The composites were fractured first in liquid nitrogen and mounted on the sample stud by means of a double-sided adhesive tape for cross-sectional view study. A thin layer of gold was sputtered onto the cross-sectional surface prior to SEM observation.

The dielectric constants of the composites were measured on a WY2851-type LCR bridge meter (Shanghai Wuyi Electronics Co., Ltd.) in the frequency range of 50 kHz to 1 MHz. The dielectric testing plates with a diameter of 30 mm and a thickness of 2 mm were obtained through cast molding. All the tests were done at room temperature and five measurements were carried out for each data point. Thermal gravimetric analysis (TGA) was carried out on a Perkin-Elmer Pyrid-1 thermal gravimetric analyzer at a heating rate of 10 °C min^{-1} from 50 to 800 °C under an N_2 atmosphere. The impact and tensile test bars were fabricated via a cast molding. Charpy impact strength was measured with a SUMITOMO impact machine tester according to a Chinese national standard of GB/T1043-98. The thickness of the Charpy impact specimen was 4 mm, and impact energy was 4 J. The tensile properties were determined with an Instron-1185 universal testing instrument using a 1000 Newton load transducer according to a Chinese national standard of GB/T1040-98. Small dumb-bell specimens with waist dimensions of 20 × 4 mm were used for tensile mechanical tests. All the tests were done at room temperature and five measurements were carried out for each data point.

Results and discussion

Microstructure and physical properties of mesoporous silicas

The SBA-15, SBA-16, and MSU-X type mesoporous silicas have a greater mesoporosity and a higher hydrothermal stability in comparison with the other type ones, indicating their significant advantage for use in the low-dielectric *o*-CNER-based composites [11, 13]. However, the commercial types of these mesoporous silicas are currently not available, so they were synthesized in our laboratory through the micelle-templating technique by seeding rod micelles of the surfactant aggregates accompanied with the condensation of a silica sol performed by the hydrolysis of TEOS. Figure 1 shows the XRD patterns of SBA-15, SBA-16, and MSU-X, and the corresponding interplanar distances for these three types of mesoporous silicas were resolved and shown in the inset of Fig. 1. Through the Bragg's law and the corresponding relationship between the cubic unit cell parameter and interplanar distance at

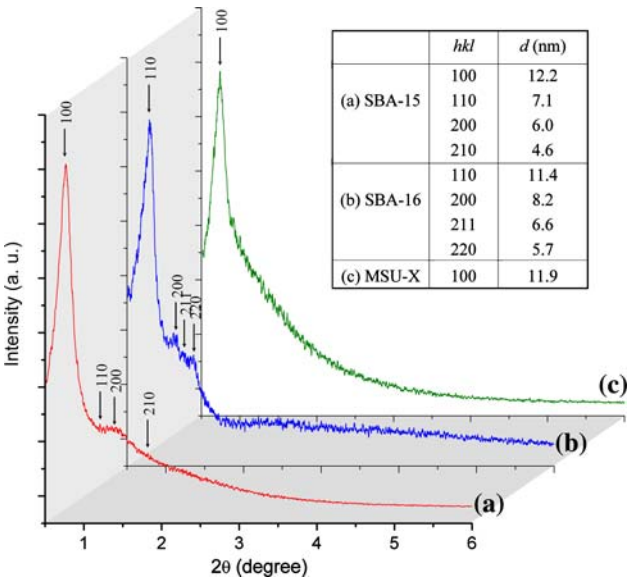

	hkl	*d* (nm)
(a) SBA-15	100	12.2
	110	7.1
	200	6.0
	210	4.6
(b) SBA-16	110	11.4
	200	8.2
	211	6.6
	220	5.7
(c) MSU-X	100	11.9

Fig. 1 X-ray diffraction patterns of the mesoporous silicas

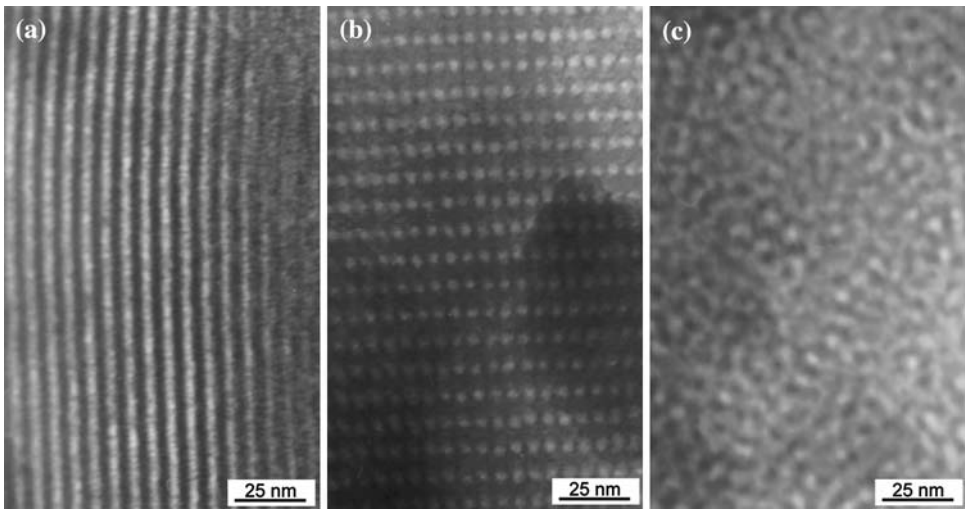

Fig. 2 TEM images of the mesoporous silicas: (**a**) SBA-15, (**b**) SBA-16, and (**c**) MSU-X

different Miller indices, a two-dimensional (2D) hexagonal structure (*p6mm*) and a 3D body-centered cubic structure (*Im3m*) could clearly be identified and assigned respectively to the SBA-15 type and the SBA-16 type mesoporous silicas. A finely resolved single diffraction peak at low 2θ angle is a typical pattern for wormhole-like mesostructures of the MSU-X type mesoporous silica [11, 23, 24].

The TEM image in Fig. 2a confirms the ordered structure of the SBA-15, and shows that the cylindrical pores are arranged in an ordered hexagonal array. From Fig. 2b, the arrays of the ordered and uniform pores interconnection can be observed for the SBA-16. The wormhole-like pores in agreement with the mesostructure of the MSU-X are also observed as shown in Fig. 2c. Nitrogen adsorption–desorption isotherms for these three types of mesoporous silicas are shown in Fig. 3. The SBA-15 exhibits a classical isotherm with H1 type vertical hysteresis loop, characteristic of cylindrical channels in good agreement with the mesostructure of the reported SBA-15. Both SBA-16 and MSU-X demonstrate a typical Langmuir IV-type isotherm with a H_2 hysteresis loop, which has a strong steep desorption branch and a sloping adsorption branch assigned to the their 3D interconnected mesoporous structure [11, 24, 25]. From the pore size distribution curves of three types of mesoporous silicas according to the analysis by using BJH method as shown in the inset of Fig. 3, it is found that these mesoporous silicas present very narrow pore size distributions with the mean pore diameters in the range of 5.3–7.4 nm. Total pore volumes for SBA-15, SBA-16, and MSU-X can also be calculated to be 1.15, 0.86, and 0.72 $cm^3\ g^{-1}$ in BET mode, which is larger than the pore volumes of typical MCM-41, about 0.57 $cm^3\ g^{-1}$ [26]. These important parameters indicate the amount of air voids stored in the mesoporous silicas [27].

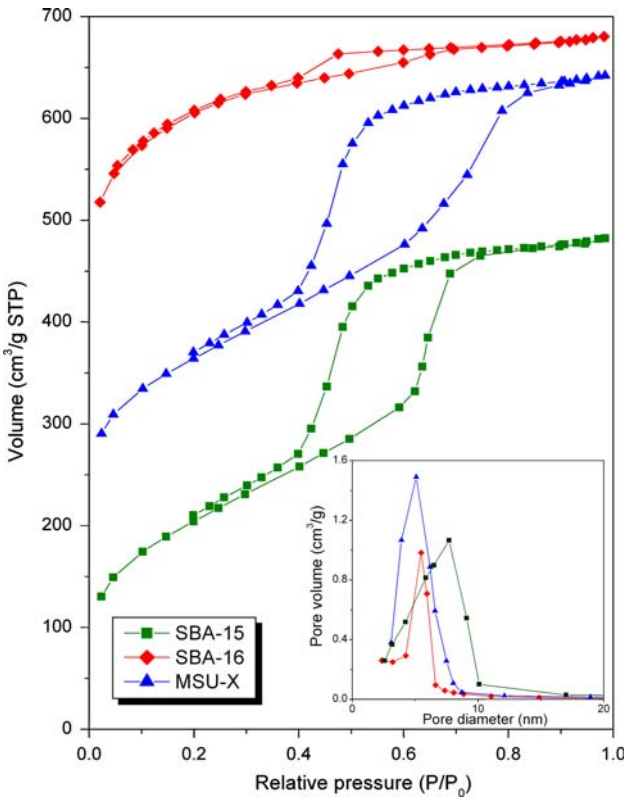

Fig. 3 N_2 adsorption–desorption isotherms and pore size distribution (the inset) plots of the mesoporous silica materials; the isotherms for MSU-X and SBA-16 are offset vertically by 120 and 320 $cm^3\ g^{-1}$ STP, respectively

Morphology

Figure 4 shows the SEM images of the microscopic morphologies for SBA-15, SBA-16, and MSU-X. It is clearly observed that the SBA-15 exhibits the long rod-like particles with a length of around 20 μm. The rod-like

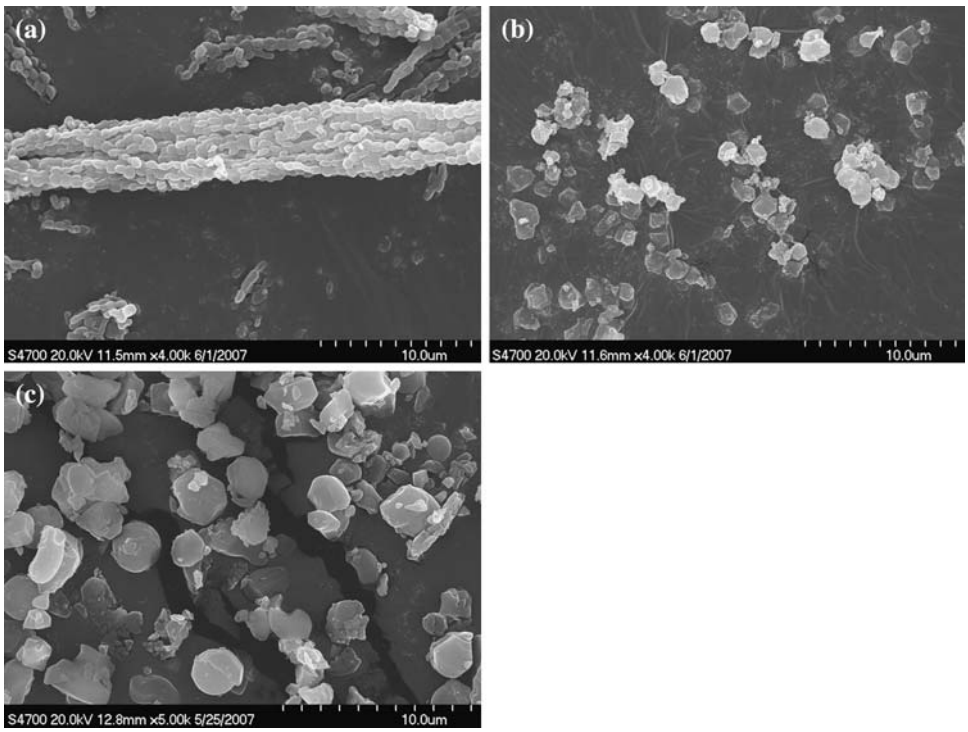

Fig. 4 SEM images of the mesoporous silicas: (**a**) SBA-15, (**b**) SBA-16, and (**c**) MSU-X

sub-particles agglomerate each other and form clusters. This is the characteristic morphology of the typical SBA-15 obtained from the condensation of TEOS around the adjacent micelles of the P123 template as previously reported [20]. It is also found from Fig. 4b, c that both SBA-16 and MSU-X present homogenous particles in random shape with a uniform size of 1–2 μm, whereas the particle size of MSU-X is larger than that of SBA-16. The original morphologies are determined by the colloidal phase separation mechanisms, which results in the different external morphologies for three types of mesoporous silicas in terms of their individual template used for synthesis [28].

The *o*-CNER/mesoporous silica composites were obtained through thermal curing of the *o*-CNER containing various amount of mesoporous silica with the MeTHPA. Owing to the poor interfacial adhesion between the inorganic mesoporous silica and the organic polymer matrix, the surface modification should first be performed for the mesoporous silica before being incorporated into the *o*-CNER. In present work, we employed the GOTMS as coupling agent, which was capable of linking mesoporous silica covalently to the cross-linking *o*-CNER molecular network during the curing reaction [29, 30]. Figure 5 shows the typical FTIR spectra of three unmodified mesoporous silicas, in which a wide absorption band at around 3,460 cm^{-1} and a weak band at 968 cm^{-1} represent Si–OH stretching and bending vibrations, respectively. Since the mesoporous silicas used in this study have been synthesized through silanol condensation in aqueous solution, the FTIR spectra confirm the existence of a large quantity of

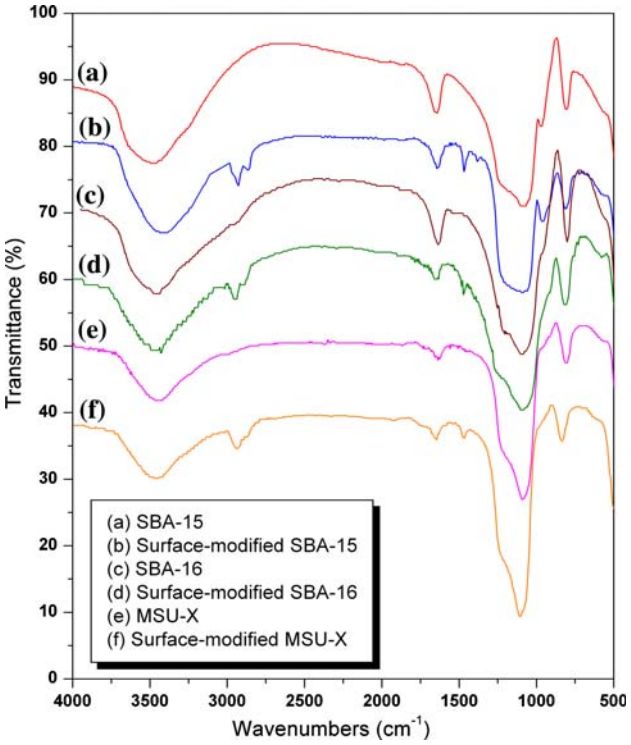

Fig. 5 FTIR spectra of the mesoporous silicas and their surface-modified products

silanol groups on their inorganic walls. Furthermore, from the IR spectra of the three surface-modified mesoporous silicas as shown in Fig. 5, a series of new absorption peaks are observed. The peak at 2,928 cm^{-1} attributed to the

–CH_2 stretching absorption, while the peaks at 2,866 and 1,465 cm^{-1} represent the –CH_2 scissor bending vibration, but the peak at 914 cm^{-1} corresponding to the absorption of the oxirane ring is overlapped by a series of intensive peaks at 838–1,094 cm^{-1} due to the absorption of the Si–O–Si and Si–OH stretching vibrations. These results indicate that the GOTMS has been chemically grafted onto the mesoporous silicas through condensation between the silanol groups of the hydrolyzed GOTMS and those on the surface of the mesoporous silica. These surface-linked GOTMS may further react with the MeTHPA during the curing process (the possible linking way is shown in Fig. 6), and thus enhance the interfacial adhesion between the mesoporous silicas and the *o*-CNER matrix.

Figure 7 shows the SEM images of the fracture surfaces of the thermosetting *o*-CNER and its composites. It is noted that the pure thermosetting *o*-CNER as a reference illustrates a glazed fracture surface with very slight plastic deformation, indicating a typical brittle fracture behavior. The mesoporous silicas dispersed in the composites can still be distinguished from the SEM images of the composites. The larger rode-like agglomeration of the SBA-15 have been broken into smaller particles, which are dispersed homogeneously as individual particles in the *o*-CNER matrix, as shown in Fig. 7a. It is also noticed that the surface of the particles attaches some resin and becomes coarse, indicating a strong interfacial adhesion as a result of the surface modification of the mesoporous silicas. The same phenomena can be observed from the fracture surfaces of the other two types composites, as shown in Fig. 7b, c. SBA-16 and MSU-X are dispersed homogeneously as individual particles in the matrix, whereas MSU-X reveals a slightly poorer dispersion than SBA-16, due to its larger particle size. However, for these two types of composites, no disengaged particles are found on the fracture surfaces, indicating a good interfacial adhesion between the mesoporous silica and the *o*-CNER matrix.

Dielectric properties

Figure 8 displays the variation of the dielectric constants measured at the frequency of 1.0 MHz as a function of the content of the mesoporous silica. The thermosetting *o*-CNER has a moderate dielectric constant of 4.0. It is noteworthy that the dielectric constants of three types of composites gradually decrease with increasing the contents of the mesoporous silica until the percentage reaches 5 wt.%, where all the composites achieve a minimum dielectric constant. After exceeding this characteristic content, the dielectric constants of all the composites begin to increase with increasing the amount of mesoporous silica continuously. Furthermore, the *o*-CNER/SBA-15 composite presents a slightly greater decrement in the dielectric constant than the *o*-CNER/SBA-16 and *o*-CNER/MSU-X ones at the characteristic content of the mesoporous silica (5 wt.%). The reason is that SBA-15 has a larger pore volume than the other ones, resulting in a greater air

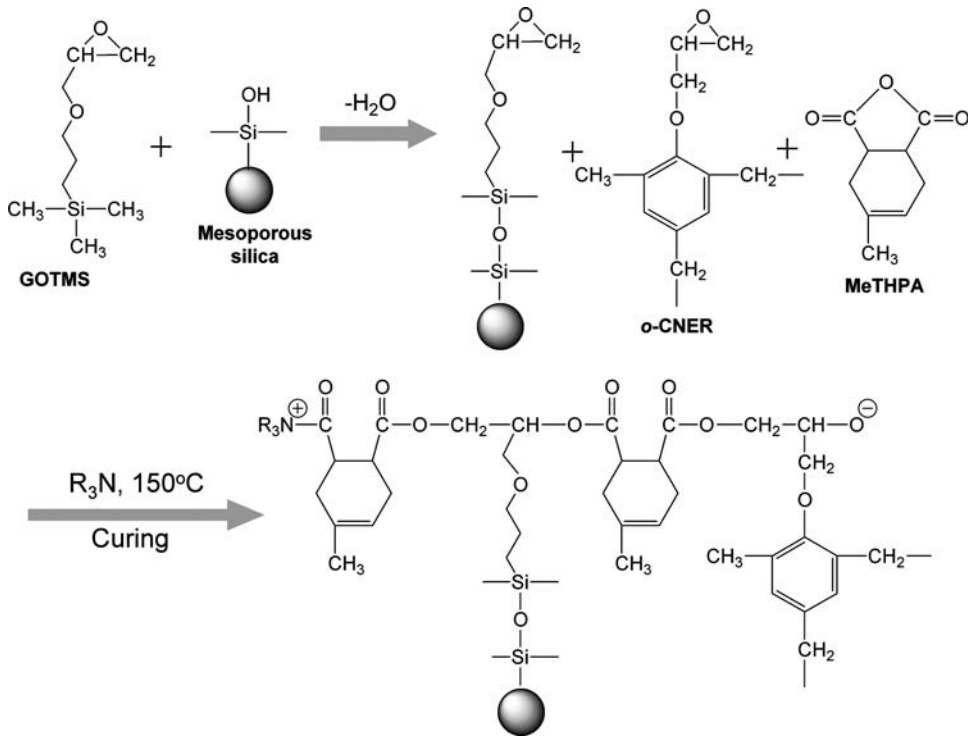

Fig. 6 Schematic linking formation of the *o*-CNER with the mesoporous silica through the interfacial reaction

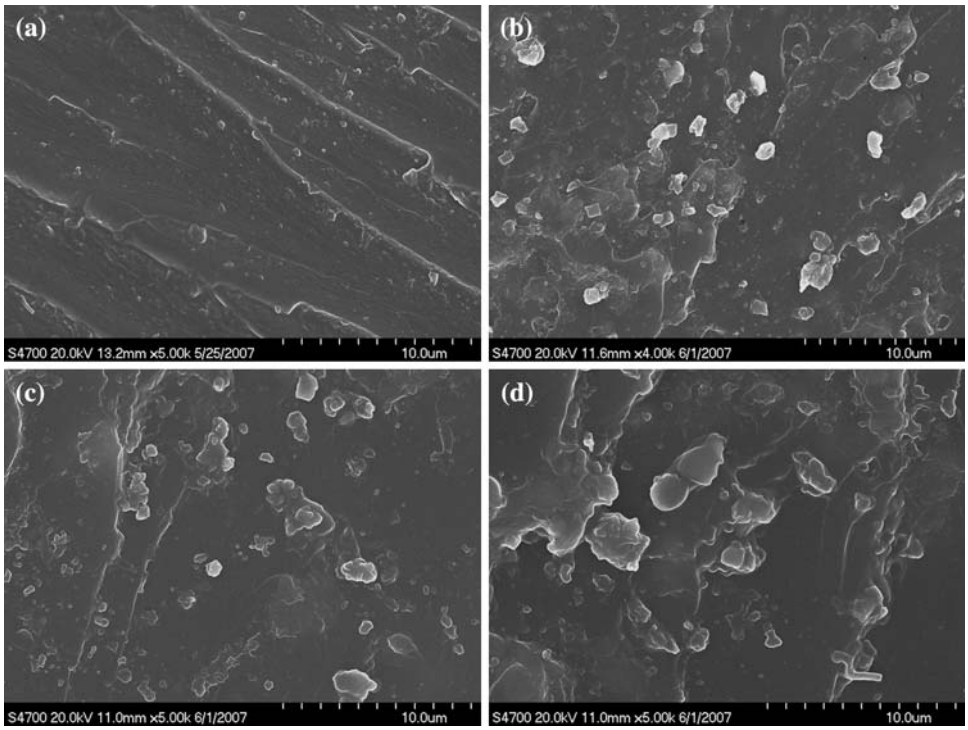

Fig. 7 SEM images of the *o*-CNER/mesoporous silica composites: (**a**) pure thermosetting *o*-CNER, (**b**) containing 7 wt.% SBA-15, (**c**) containing 7 wt.% SBA-16, and (**d**) containing 7 wt.% MSU-X

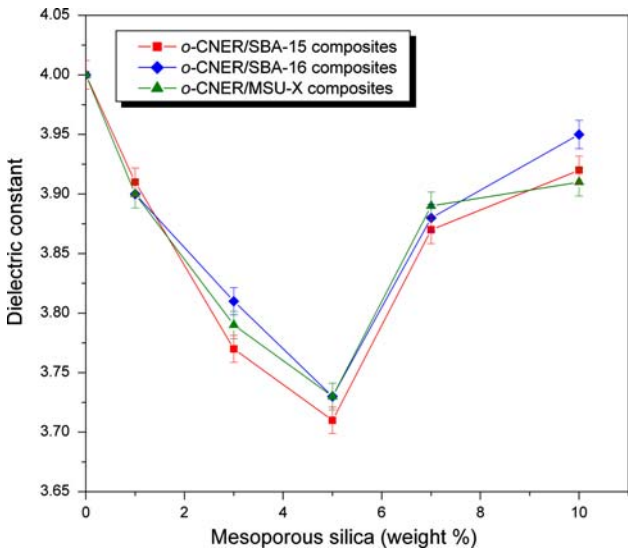

Fig. 8 Dielectric constants of the *o*-CNER/mesoporous silica composites at a frequency of 1.0 MHz as a function of the content of the mesoporous silica

stored within it. All of the measurements have been repeated five times and the deviations of the testing data were controlled with ±0.03. Therefore, it is believable that the reduction of the dielectric constant results from the incorporation of air voids ($c = 1$) when the mesoporous silica is introduced into the composites.

As we know, there are mainly three models that can be used to predict the dielectric constant of the dual-component composite: Maxwell–Garnett, Bruggeman, and Yamada models. The Maxwell–Garnett equation was widely used to calculate the dielectric constant of polymeric composites [31, 32]. The Yamada model was mainly used to calculate the dielectric constant at different electric field strengths, so the depolarization factor should be considered based on the electric field effect with a complicated equation [33]. The Yamada model is outside of the target of our research on the *o*-CNER/mesoporous silica composites. Although there are three components including *o*-CNER, silica (SiO_2), and air in the composites, the reduction of the dielectric constant is mainly attributed to the implantation of air alone with the mesoporous silicas. Therefore, the composite can be first considered as a dual-component system (the *o*-CNER and the mesoporous silica). The theoretic dielectric constants of the composites can be predicted by using the Maxwell–Garnett equation [32]:

$$\frac{c - c_e}{c + 2c_e} = \phi_m \frac{c_m - c_e}{c_m + 2c_e} \quad (1)$$

where c_e and c_m are the dielectric constants of the thermosetting *o*-CNER and the mesoporous silica, respectively, c the predicted dielectric constant of the composite, and ϕ_m the volume fraction of the mesoporous silica. The dielectric constants of the three types of mesoporous silicas were also calculated by Eq. 1 based on the total pore volume, corresponding to the air volume stored within mesoporous silica. All of the calculated dielectric constants as well as the measured ones for reference are listed in Table 1. It is noticed that the measured dielectric constants of the

Table 1 Measured and theoretical dielectric constants, and air volume percentages in the thermosetting *o*-CNER and its composites with mesoporous silicas calculated by corresponding models

Materials	Measured dielectric constant at 1 MHz	Theoretical dielectric constant[a]	Air volume stored within mesoporous silica in composites[b] (v./v.%)	Total air volume in composites[c] (v./v.%)
o-CNER	4.00	–	–	–
Silica (SiO_2)	4.00	–	–	–
Air	1.00	–	–	–
o-CNER/1 wt.% SBA-15	3.91	3.94	1.03	2.26
o-CNER/3 wt.% SBA-15	3.77	3.82	3.01	5.79
o-CNER/5 wt.% SBA-15	3.71	3.72	4.89	7.31
o-CNER/7 wt.% SBA-15	3.87	3.63	6.68	–
o-CNER/10 wt.% SBA-15	3.92	3.49	9.21	–
o-CNER/1 wt.% SBA-16	3.90	3.97	0.91	2.51
o-CNER/3 wt.% SBA-16	3.81	3.91	2.71	4.78
o-CNER/5 wt.% SBA-16	3.73	3.86	4.47	6.80
o-CNER/7 wt.% SBA-16	3.88	3.80	6.20	–
o-CNER/10 wt.% SBA-16	3.95	3.72	8.72	–
o-CNER/1 wt.% MSU-X	3.90	3.95	0.96	2.51
o-CNER/3 wt.% MSU-X	3.79	3.88	2.85	5.28
o-CNER/5 wt.% MSU-X	3.73	3.81	4.67	6.80
o-CNER/7 wt.% MSU-X	3.89	3.73	6.43	–
o-CNER/10 wt.% MSU-X	3.91	3.63	8.99	–

[a] The theoretical dielectric constants were calculated by using Maxwell–Garnett equation

[b] The air volume stored within the mesoporous silica in the composites (volume fraction) was calculated by using the data from the N_2 adsorption–desorption measurements

[c] Total air volume in the composites (volume fraction) was calculated according to Bruggeman's model

composites are different from the theoretic data that are slightly greater at the same amount of the mesoporous silica. The results show that the difference of the pore volumes in the mesoporous silica exactly plays an important role to decrease the dielectric constants of the composites. Furthermore, the theoretic data decrease continuously with increasing the amount of the mesoporous silica, but the measured values present a minimum at a characteristic content of the mesoporous silica. This implies that the reduction of the dielectric constants is not completely attributed to the air volume stored within the mesoporous silicas.

In order to explore the reason why this deviation occurs, we calculated the air volume percentages of the composite by only considering the air volume within the mesoporous silicas obtained from the N_2 adsorption–desorption measurement, and the total air volume in the composite by using Bruggeman's model. Assuming there are only three phases in the composite as mentioned previously, the total volume percentages in the composite is calculated by using Bruggeman's equation [34] for three-component system:

$$\phi_e\left(\frac{c_e - c}{c_e + 2c}\right) + \phi_s\left(\frac{c_s - c}{c_s + 2c}\right) + \phi_a\left(\frac{c_a - c}{c_a + 2c}\right) = 0 \qquad (2)$$

where c_e, c_s, and c_a are the dielectric constants of the thermosetting *o*-CNER, silica, and air, respectively, c the measured dielectric constant of the composite, and ϕ_e, ϕ_s, and ϕ_a the volume fractions of the thermosetting *o*-CNER, silica and air, respectively. The calculated results are also listed in Table 1. It is clearly found that the actual total air volume in the composite is much greater than the air volume stored within mesoporous silica. The air voids may exist in the gaps on the interface between the mesoporous silica and the *o*-CNER matrix, and the free volume created by introducing macro-sized domains [35]. From Fig. 8, it is found that the air voids exist exactly around the mesoporous silica and decrease the dielectric constant of the composites drastically. Moreover, the air volume in the pores created during mixing process should also be considered as contribution to the total air volume. Therefore, the reduction of dielectric constant is contributed by the whole air voids created by incorporating the mesoporous silica, which include the air volume stored within the mesoporous silica, the air void coming from the gaps on the interface between the mesoporous silicas and the *o*-CNER matrix, and the free volume created by introducing macro-sized domains. The total air volume presents a maximum at a characteristic content of the mesoporous silica and begins to decrease with increasing the amount of the mesoporous silica continuously in terms of the Bruggeman's model. This indicates that incorporating too much mesoporous silica results in an aggregation and a poor dispersion, which causes a decrease of the air volume, and thus an increase of the dielectric constant.

Figure 9 shows the frequency dependence of dielectric constant of the thermosetting *o*-CNER and its composites

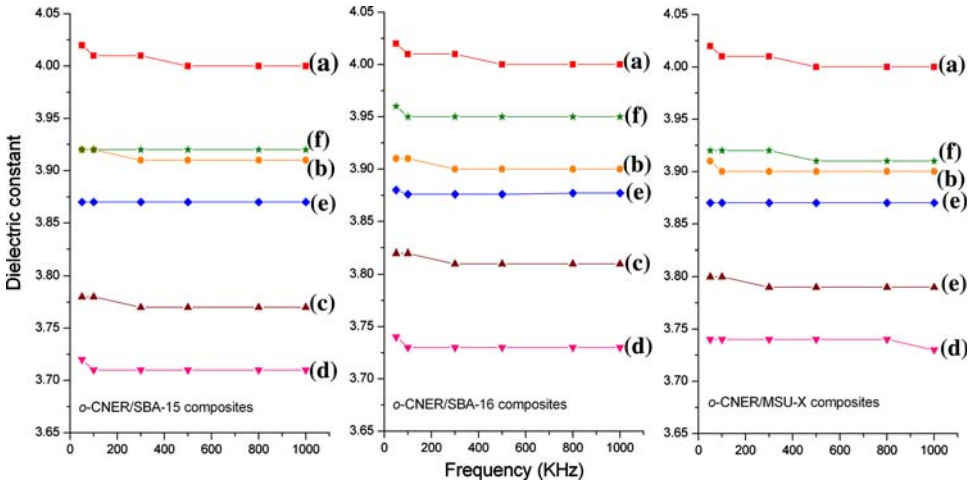

Fig. 9 Frequency dependence of dielectric constants of the *o*-CNER/mesoporous silica composites containing (**a**) 0 wt.%, (**b**) 1 wt.%, (**c**) 3 wt.%, (**d**) 5 wt.%, (**e**) 7 wt.%, and (**f**) 10 wt.% mesoporous silica

in the frequency range of 50–1,000 kHz. Although the variation of the dielectric constants of the composites as a function of the content of the mesoporous silica is identical to the trend shown in Fig. 8, the dielectric constants for both pure *o*-CNER and its composites are almost independent of the frequency except at very low frequency, where some dielectric constants are fairly higher. The dielectric constant only decreases slightly with increasing frequency while the temperature keeps constant at room temperature. It is well known that the dielectric constants of materials tend to decrease gradually with increasing the frequency, because the response of the electronic, atomic, and dipolar polarizable units varies with frequency. This behavior can be attributed to the frequency dependence of the polarization mechanisms [36]. Therefore, the magnitude of the dielectric constant for a polymer like *o*-CNER is determined by the ability of the polarizable units to orient fast enough to keep up with the applied alternating current electric field. The orientational polarization decreases while the frequency increases, as the orientation of dipole moments needs a longer time than the electronic and ionic polarization. This results in a reduction of the dielectric constant. The *o*-CNER/mesoporous silica composites prepared in the present work exhibit the stable dielectric constants across the wide frequency range, which are highly preferred for many microelectronic applications.

Thermal properties

Effects of the three types of mesoporous silicas on the thermal degradation of the *o*-CNER were studied using TGA in the temperature range of 50–800 °C, and the TGA thermograms are shown in Fig. 10. The thermal degradation of the thermosetting *o*-CNER and its composites occurs through one degradation step in this temperature range, indicating a good phase interconnection between the mesoporous silica and the *o*-CNER matrix, and successful

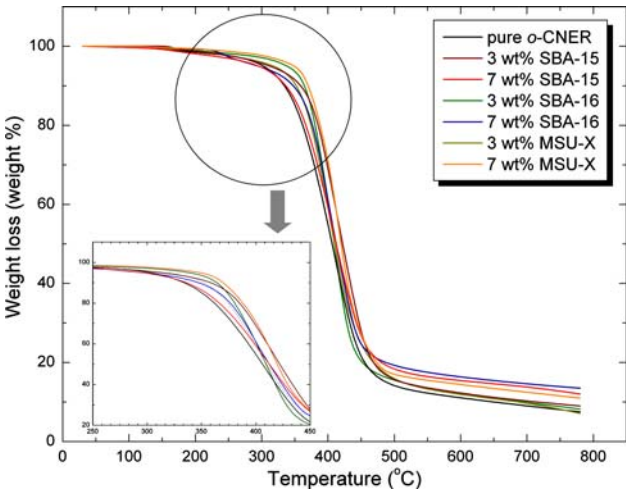

Fig. 10 TGA thermograms of the thermosetting *o*-CNER and its composites with the mesoporous silicas

chemical graft of the GOTMS onto the mesoporous silicas. The TGA thermograms also suggested that water or solvent has been successfully removed from the resins and the composites, because there is no weight loss below 100 °C. It is clearly demonstrated in Fig. 10 that the thermal stability of the *o*-CNER is improved by incorporation of the mesoporous silica in terms of the temperatures at the rapid weight loss and the weight percent of the residues above 700 °C. The improvement in these two parameters suggests that the incorporation of the mesoporous silica into the *o*-CNER results ultimately in an improvement in thermal stability. This improvement in the thermal stability mainly comes from the enhanced interaction between the *o*-CNER and the mesoporous silica through chemical bonding [37]. Furthermore, it may also be assumed that the thermal stability of organic materials can be improved by introducing inorganic components like silica, on the basis of the fact that these materials have inherently good thermal stability [38].

Mechanical properties

The impact strength, tensile strength, and elongation at break of the *o*-CNER/mesoporous silica composites as a function of the content of the mesoporous silica materials are displayed in Figs. 11–13, indicating that the incorporation of mesoporous silica materials has significant effects on the mechanical properties. The thermosetting *o*-CNER suggests a typical brittle plastic behavior with low impact strength of 4.3 kJ m^{-2} and a high tensile strength of 87.7 MPa. It is noteworthy that the impact strength of the three types of composites all increases with introducing 1 wt.% mesoporous silica into the *o*-CNER, and reach a maximum value with addition of 3 wt.% mesoporous silica. It is evident that the toughening effect of the mesoporous silica materials could be explained by the crack front bowing mechanism [39, 40]. For the toughening polymer system using inorganic particles, the rigid particles can resist the propagation of the crack, so the primary crack has to bend between the neighboring particles. However, the impact strength begins to decrease, as the weight percent of mesoporous silica increases continuously, suggesting that the high concentration of mesoporous silica dominates the natural incompatibility of the inorganic and organic phases, and thus results in a reduction in toughness [41]. Furthermore, the tensile strength and elongation at break also decrease rapidly with incorporation of the mesoporous silica (see Figs. 12 and 13). This is a result of the natural incompatibility between the inorganic silica and the organic *o*-CNER, leading to a poor stress transfer. On the other hand, although the mechanical properties of the three types of composites present similar trend of variation as a function of composition of the mesoporous silica, the *o*-CNER/SBA-15 composites indicate a much better toughening effect and a less deterioration of the tensile properties than the other two ones, due to the much smaller particle size of SBA-15.

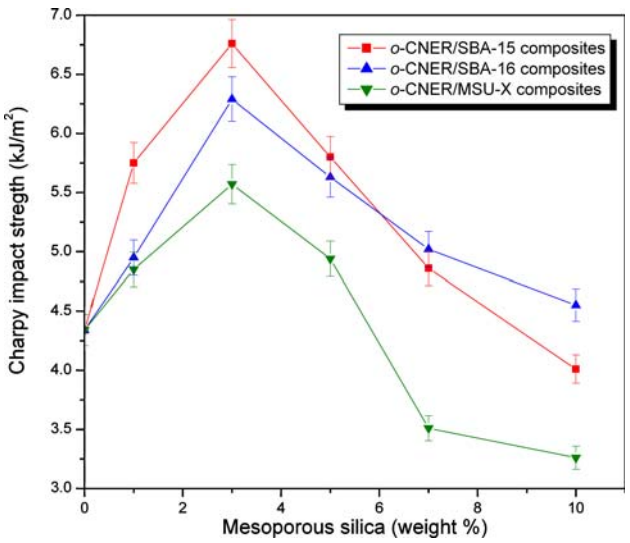

Fig. 11 Impact strength of the *o*-CNER/mesoporous silica composites as a function of the content of the mesoporous silicas

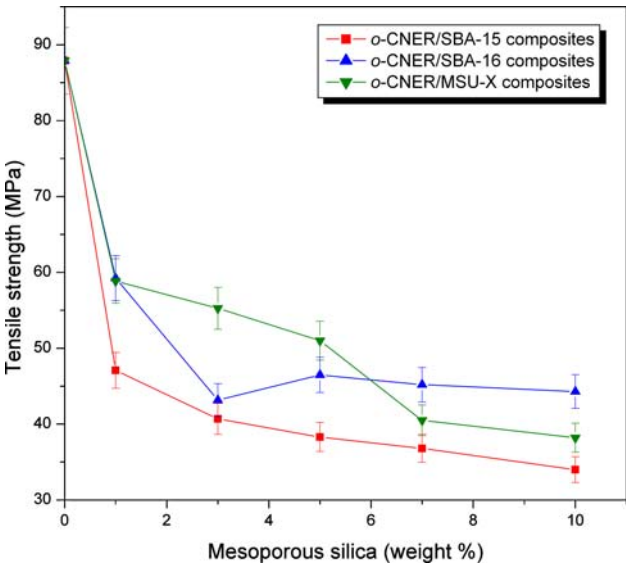

Fig. 12 Tensile strength of the *o*-CNER/mesoporous silica composites as a function of the content of the mesoporous silicas

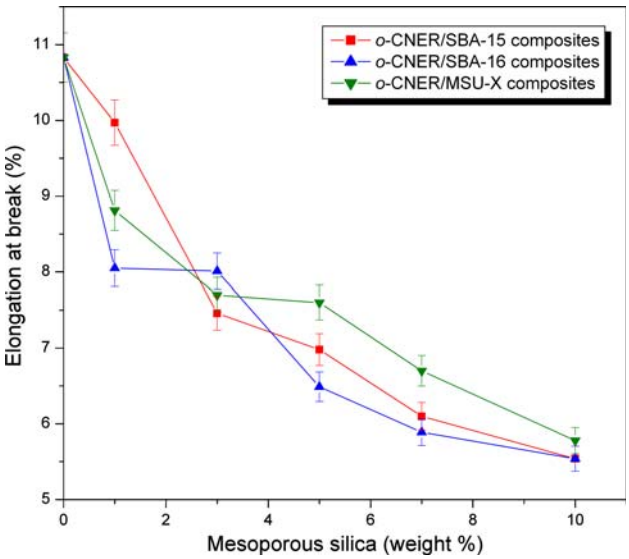

Fig. 13 Elongation at break of the *o*-CNER/mesoporous silica composites as a function of the content of the mesoporous silicas

Conclusion

The *o*-CNER composites containing various amount of SBA-15, SBA-16, and MSU-X were successfully prepared through thermal curing with MeTHPA. The dielectric constants of the *o*-CNER/mesoporous silica composites can

be reduced from 4.0 of the pure *o*-CNER to around 3.7 by incorporation of 5 wt.% mesoporous silicas. The reduction of the dielectric constant is attributed to the incorporation of the air voids ($c = 1$) stored within the mesoporous silicas, the air volume existing in the gaps on the interfaces between the mesoporous silica and the *o*-CNER matrix, and the free volume created by introducing large-sized domains. SBA-15 has a more significant effect on reduction of the dielectric constant than the other ones because of its larger pore volume. The *o*-CNER/mesoporous silica composites also present a good phase interconnection and stable dielectric constants across the wide frequency range. The thermal stability of *o*-CNER can be improved by incorporation of the mesoporous silicas. The incorporation of the mesoporous silicas is a promising approach to reduce the dielectric constant of the epoxy resins. The enhanced interfacial interaction between the surface-modified mesoporous silica and the *o*-CNER matrix can also lead to the improvement of the toughness. The incorporation of the mesoporous silica materials is a promising approach to reduce the dielectric constant of the epoxy resins.

Acknowledgements The authors greatly appreciate financial support from the National Natural Science Foundation of China (Grant No.: 50573006).

References

1. Wong CP, Wong MM (1999) IEEE T Compon Pack T 22:21. doi:10.1109/6144.759349
2. Enlow LR, Swanson DW, Naito CM (1999) Microelectron Reliab 39:515. doi:10.1016/S0026-2714(98)00202-9
3. Tai HJ, Wang JB, Chen JH et al (2001) J Appl Polym Sci 79:652. doi:10.1002/1097-4628(20010124)79:4<652::AID-APP90>3.0.CO;2-U
4. Kim WG, Lee JY (2002) Polymer 43:5713. doi:10.1016/S0032-3861(02)00444-5
5. Imai T, Sawa F, Nakano T et al (2006) IEEE T Dielect El In 13:319. doi:10.1109/TDEI.2006.1624276
6. Flandin L, Vouyovitch L, Beroual A et al (2005) J Phys D Appl Phys 38:144. doi:10.1088/0022-3727/38/1/023
7. Han JT, Cho KW (2005) Macromol Mater Eng 290:1184. doi:10.1002/mame.200500051
8. Gao JG, Zhao M, Li G (2006) J Appl Polym Sci 101:3023. doi:10.1002/app.23670
9. Liu YL, Chen CP, Jeng RJ (2003) J Appl Polym Sci 90:4047. doi:10.1002/app.13159
10. Yang PD, Zhao DY, Margolese DI et al (1998) Nature 396:152. doi:10.1038/24132
11. Zhao DY, Feng JL, Huo QS et al (1998) Science 279:548. doi:10.1126/science.279.5350.548
12. Zhao D, Yang P, Melosh N et al (1998) Adv Mater 10:1380. doi:10.1002/(SICI)1521-4095(199811)10:16<1380::AID-ADMA1380>3.0.CO;2-8
13. Baskaran S, Liu J, Domansky K et al (2000) Adv Mater 12:291. doi:10.1002/(SICI)1521-4095(200002)12:4<291::AID-ADMA291>3.0.CO;2-P
14. Yang CM, Cho AT, Pan FM et al (2001) Adv Mater 13:1099. doi:10.1002/1521-4095(200107)13:14<1099::AID-ADMA1099>3.0.CO;2-0
15. Wang J, Zhang CR, Feng J (2005) Prog Chem 17:1001
16. Chen-Yang YW, Chen CW, Wu YZ et al (2005) Electrochem Solid-State Lett 8:F1. doi:10.1149/1.1825311
17. Lin JJ, Wand XD (2007) Polymer 48:318. doi:10.1016/j.polymer.2006.10.037
18. Cheng CF, Cheng HH, Cheng PW et al (2006) Macromolecules 39:7583. doi:10.1021/ma060990u
19. Wang N, Zhang J, Dai CY et al (2006) Eng Plast Appl 34:15
20. Zhao D, Sun J, Li Q et al (2000) Chem Mater 12:275. doi:10.1021/cm9911363
21. Jin ZW, Wang XD, Cui XG (2008) Microporous Mesoporous Mater 108:183
22. Jin ZW, Wang XD, Cui XG (2008) J Non-Cryst Solids 353:2507. doi:10.1016/j.jnoncrysol.2007.05.003
23. Zhao DY, Huo QS, Feng JL et al (1998) J Am Chem Soc 120:6024. doi:10.1021/ja974025i
24. Prouzet E, Boissiere C, Patricia JK (2002) J Mater Chem 12:1553. doi:10.1039/b111236h
25. Morishige K, Tateishi N, Fukuma S (2003) J Phys Chem B 107:5177. doi:10.1021/jp022137c
26. Khodakov AY, Zholobenko VL, Bechara R et al (2005) Microporous Mesoporous Mater 79:29. doi:10.1016/j.micromeso.2004.10.013
27. Shi YF, Meng Y, Chen DH et al (2006) Adv Funct Mater 16:561. doi:10.1002/adfm.200500643
28. Yu CZ, Fan J, Tian BZ et al (2004) Chem Mater 16:889. doi:10.1021/cm035011g
29. Mascia L, Prezzi L, Haworth B (2006) J Mater Sci 41:1145. doi:10.1007/s10853-005-3653-5
30. Zunjarrao SC, Singh RP (2006) Compos Sci Technol 66:2296. doi:10.1016/j.compscitech.2005.12.001
31. Kutnjak Z, Vodopivec B, Kuscer D (2005) J Non-Cryst Solids 351:1261. doi:10.1016/j.jnoncrysol.2005.02.016
32. Hernandez-Torres J, Mendoza-Galvan A (2005) J Non-Cryst Solids 351:2029. doi:10.1016/j.jnoncrysol.2005.05.011
33. Yamada T, Uead T, Kitayama T (1982) J Appl Phys 53:4328. doi:10.1063/1.331211
34. Zhang YH, Lu SG, Li YQ et al (2005) Adv Mater 17:1056. doi:10.1002/adma.200401330
35. Wahab MA, Kim I, Ha CS (2003) Polymer 44:4705. doi:10.1016/S0032-3861(03)00429-4
36. Deligoz H, Yalcinyuva T, Ozgumus S, Yildirim S (2006) J Appl Polym Sci 100:810. doi:10.1002/app.23174
37. Choi MH, Chung IJ (2003) J Appl Polym Sci 90:2316. doi:10.1002/app.12763
38. Dean K, Krstina J, Tian W et al (2007) Macromol Mater Eng 292:415. doi:10.1002/mame.200600435
39. Bartczak Z, Argon AS, Cohen RE et al (1999) Polymer 40:2347. doi:10.1016/S0032-3861(98)00444-3
40. Thio YS, Argon AS, Cohen RE et al (2002) Polymer 43:3661. doi:10.1016/S0032-3861(02)00193-3
41. Argon AS, Cohen RE (2003) Polymer 44:6013. doi:10.1016/S0032-3861(03)00546-9